Competition between particle formation and burrowing: Gold on bismuth

P. Swaminathan, J. S. Palmer, and J. H. Weaver
Department of Materials Science and Engineering, University of Illinois at Urbana-Champaign, Urbana, Illinois 61801, USA
(Received 14 March 2008; revised manuscript received 18 July 2008; published 17 September 2008)

We discuss Au vapor deposition on polycrystalline Bi under conditions where particle formation and burrowing are competitive. Burrowing occurs because the surface free energy of Bi is lower than that of Au, the Au-Bi interface energy is small, and the kinetics, in terms of high surface and grain boundary diffusion rates, are favorable. For formation of Au particles on Bi, kinetic Monte Carlo simulations that include the relative rates of atom impingement, surface diffusion, and burrowing show a broadening of the overall size distribution. This occurs because burrowing continuously removes small particles from the surface, reduces the density of existing nuclei, and allows those that remain to grow by atom capture to larger sizes before they too are completely burrowed. These results are important for systems where nanostructures are assembled on low surface energy substrates.

DOI: 10.1103/PhysRevB.78.115416 PACS number(s): 61.46.−w, 68.37.−d, 68.55.A−, 68.43.Jk

I. INTRODUCTION

Island formation caused by atomic diffusion on surfaces has been extensively studied using a host of experimental and theoretical techniques.[1–3] The effects of arrival rate, adatom and small cluster diffusion, island coalescence, and coverage have been studied. These results help us understand the formation of supported three-dimensional nanostructures.[4]

The lowest-energy configuration for a crystalline nanometer-sized particle on a substrate with a lower surface energy and minimal interface energy would be reached if it were embedded within the host, not supported by it. This would be achieved by particle burrowing, and it would be driven by capillary forces. Capillary forces would cause substrate atoms to move along the particle-substrate interface and allow the particles to sink. For kinetic reasons, extensive burrowing is infrequently observed.[5] However, it has been observed for Co particles deposited at 330 °C on Cu and Ag,[5] as evidenced from atomic force microscopy and cross-sectional transmission electron microscopy (TEM) images, and for Co particles on Au after annealing at 180 °C.[6] Other studies of metals with a higher surface energy than the substrate have shown a monolayer or bilayer of the substrate coating the particles (surfactant effect), e.g., Ni/Ag (Ref. 7) and Rh/Ag.[8] A surfactant effect was observed during Au deposition on 1 ML of Bi on Au (111) surfaces.[9] Auger analysis showed that at room temperature the Bi is segregated to the top. Bi has also been used as a surfactant for homoepitaxial growth of Fe and Cr.[10,11]

In this paper, we focus on the Au/Bi system where burrowing is thermodynamically favorable. This system was chosen because the low melting temperature of Bi, 272 °C, leads to high surface and grain boundary diffusivities. The equilibrium Au-Bi phase diagram shows negligible solid solubility until ~120 °C, when an Au_2Bi phase forms. Hence, we can neglect any alloying or solubility effects at room temperature.[12] Solubility effects might become important for growth close to the phase-transition temperature. We show that burrowing is kinetically competitive with the nucleation and growth of Au particles by atom impingement and diffusion. As depicted in Fig. 1, the early Au nuclei are stable and there is minimal solid solubility at room temperature. With increased deposition, however, these nuclei grow into three-dimensional particles, for which the concepts of surface and interface energies take on meaning, and this initiates burrowing. We have used TEM to study the consequences of such burrowing, varying the temperature during deposition to alter the kinetics of diffusion and burrowing. What is novel is that burrowing occurs during atom deposition and it removes particles from the surface. This forces nucleation of new particles and also allows particles that are partially burrowed to grow to larger sizes than would normally be observed. Kinetic Monte Carlo simulations of particle formation, with a burrowing component, show how the overall size distribution is affected by the rate of atom arrival, atom diffusion, and particle burrowing.

II. EXPERIMENTAL DETAILS

Growth was performed in a vacuum chamber with a base pressure below 1×10^{-9} Torr. The substrates were amorphous carbon (a-C) TEM grids degassed at 400 °C for 5 min and then subsequently heated during the chamber bake. Bi films were grown at room temperature by vapor deposition at a rate of ~1 nm/min. The films were polycrystalline and characterized by x-ray and electron diffraction. X-ray dif-

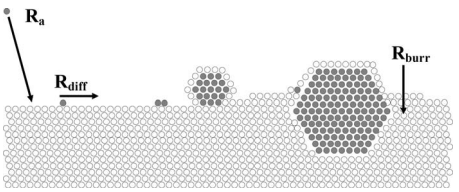

FIG. 1. Schematic of Au particle formation and burrowing in a (001) Bi grain. A particle burrows by displacing atoms, driven by capillary forces, which depend on the particle size as it grows from a cluster to a nanocrystal with distinct surface energies. The final size and distribution depends on the relative rates of the adatom impingement (R_a), diffusion (R_{diff}), and the particle burrowing rate (R_{burr}). A partially buried particle can grow by adatoms attaching to it, while one that is completely buried cannot.

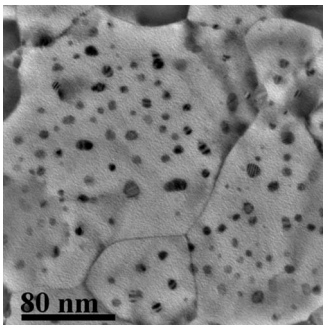

FIG. 2. Typical plan view TEM image of nanoparticles formed when 5 Å of Au was deposited on a 20-nm Bi film at room temperature. Fringes seen in some particles are Moiré patterns due to interference between the Au and Bi lattices. They can be used to determine the orientation of the particles.

fraction (XRD) spectra were recorded on a Rigaku D-Max instrument. The film thicknesses were varied from 10–30 nm to check the effects of grain size on particle formation. Au was vapor deposited at a rate of ~1 Å/min with the substrates held at 25, 50, 75, and 100 °C. Average particles sizes and size distributions were obtained using a 120 keV Philips CM 12 TEM. Cross-sectional images were obtained by using a sharp tip to break areas in the grid and imaging the cross section of the free standing film areas. Cross-sectional images were recorded in a 200 keV JEOL 2010 LaB_6 TEM.

III. RESULTS AND DISCUSSION

A. Particle morphology and burrowing

Bi grows by island formation on a-C at room temperature, and these islands grow together to form polycrystalline films. XRD measurements indicate preferential growth of (001) type grains with vertical grain sizes equal to the film thickness. TEM images show that lateral grain sizes are 3–4 times the film thickness. These results are consistent with normal grain growth at temperatures greater than half the melting point.[13]

Mobile Au atoms on the Bi films form nuclei and ultimately particles at room temperature. Figure 2 is a representative plan view TEM image of those formed by depositing 5 Å of Au on a 20-nm Bi film. The average particle radius was 3.5 ± 1.1 nm, corresponding to ~10,000 atoms. The average particle density was $1.6 \pm 0.4 \times 10^{11}$ cm^{-2}. Size distributions and densities do not change with Bi film thickness in the range 10–30 nm. Hence, effects such as Au atom trapping at grain and triple boundaries can be neglected. The particles are stable during imaging and over time, indicating that they do not undergo any postdeposition growth or ripening. Although randomly oriented, some show Moiré patterns with bright and dark fringes that arise from the interference between the Au and Bi lattices. They can be used to deduce the Au particle orientations.[14] Figure 3 shows cross-sectional images of Au particles buried in Bi films of thicknesses 10 and 30 nm. A high-resolution image of the boxed particle in Fig. 3(b) is shown in Fig. 3(c), where the lattice fringes in the Au particle and Bi film are seen clearly. Based on these cross-sectional images we conclude that the particles seen in plan view of Fig. 2 are actually buried in the film. It also indicates that they are approximately equiaxed. In TEM, particles within or supported by a film would be visible as long as the contrast exists. To check this assertion, we formed Au particles by directly depositing onto a-C and then grew Bi films on top of the particles. The Au particles were still visible for film thicknesses of 10 nm. Since, in our burrowing experiments the particles are close to the surface they would still be visible.

Epitaxial particles have a slower burrowing rate than nonaligned ones.[15] For systems with small lattice mismatch, such as Co on Cu (lattice mismatch <2%), particles rotate to align with the film and this process slows the burrowing rate. For Au on Bi, the smallest lattice mismatch occurs when the Moiré patterns are visible, namely, 4%. This is high enough to ignore any rotation of the particles, and we can consider the burrowing to be independent of the particle morphology.

Burrowing can be seen to be favorable by considering the energy reduction when a particle sinks into the film, namely,[5]

$$\Delta\gamma = (\gamma_{\mathrm{Bi}} + \gamma_{\mathrm{Au\text{-}Bi}} + \gamma_{\mathrm{chem}}) - \gamma_{\mathrm{Au}}, \quad (1)$$

where γ_{Bi} and γ_{Au} are the surface free energies of Bi and Au, respectively. Calculations using density-functional theory give 0.53 J m^{-2} for Bi (001) and 1.28 J m^{-2} for Au (111).[16]

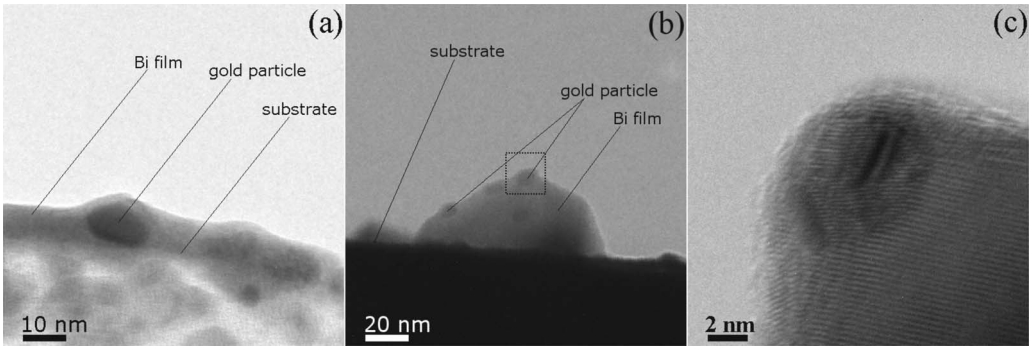

FIG. 3. Cross-sectional TEM images of Au particles buried within Bi films of thicknesses (a) 10 and (b) 30 nm. The images were obtained by breaking areas in the deposited film using a sharp tip and imaging portions of the free standing film that were oriented favorably. The particles were obtained by depositing 5 Å Au. In plan view, the particles look like those in Fig. 2. (c) A high-resolution TEM image of the boxed area in (b), showing a single particle of Au in Bi with the lattice fringes in Au and Bi clearly visible.

The interface energy, $\gamma_{\text{Au-Bi}}$, can be approximated as the average of the high angle grain boundary energies of the two species. Using 0.15 J m^{-2} and 0.4 J m^{-2} for Bi (Ref. 17) and Au (Ref. 18), respectively, we obtain $\gamma_{\text{Au-Bi}}$ =0.28 J m^{-2}. γ_{chem} represents the immiscibility between the two components; it is the product of the heat of mixing, 650 J mol^{-1},[12] and the areal density of atoms at the surface, 10^{19} m^{-2}. This gives $\Delta\gamma$=−0.46 J m^{-2}, a substantial energy reduction by burrowing.

B. Kinetics of burrowing

Burrowing is a continuous process and occurs for as long as the driving force, the lowering of the particle free energy, is present. Only when the particle is completely covered by the film does burrowing stop. The rate at which it occurs is dictated by kinetics. To estimate burrowing times, we can use an expression derived by Zimmermann *et al.*[19] for Co particles on Cu, namely,

$$t = \alpha \frac{kT}{V_m \gamma_{\text{Bi}} \delta D} r^4, \tag{2}$$

where α is a geometric factor that has a value of 1.1 when the particle is submerged in the film. k, r, and T represent the Boltzmann factor, particle radius, and temperature, respectively. V_m is the volume of one Bi atom, γ_{Bi} is the surface free energy of Bi, and δD represents diffusion of the Au/Bi interface, given by the geometric mean of the grain boundary self-diffusion coefficients,[20]

$$\delta D = \sqrt{\delta D_{\text{Au}} \delta D_{\text{Bi}}},$$

$$\delta D_{\text{Au}} = 1.9 \times 10^{-16} \exp\left(-10 \frac{T_{m(\text{Au})}}{T}\right) \text{m}^3\ \text{s}^{-1},$$

$$\delta D_{\text{Bi}} = 2.7 \times 10^{-14} \exp\left(-11 \frac{T_{m(\text{Bi})}}{T}\right) \text{m}^3\ \text{s}^{-1}, \tag{3}$$

where $T_{m(\text{Au/Bi})}$ is the bulk melting point. The calculations indicate that the burrowing time, at room temperature, varies from a few seconds for a 1-nm particle to ~30 min for the ones with a radius of 4 nm.

To verify the calculations for the burrowing time, we divided the deposition into two segments of 2.5 Å each, with a pause between them to allow the first batch to burrow. Figures 4(a) and 4(d) show the size distributions obtained by depositing 5 Å and 2.5 Å Au at a rate of ~1 Å/min. Figures 4(b) and 4(c) show the distributions when there was a pause of 2 and 30 min, respectively, between two depositions of 2.5 Å. Comparison of Figs. 4(a) and 4(c) suggests that most of the particles that formed during the first 2.5 Å deposition, and having the size distribution given by Fig. 4(d), had burrowed in 30 min. Only the larger particles were not fully burrowed, as depicted in Fig. 1, and they grew by adatom capture. Thus, the difference in the size distributions in Figs. 4(c) and 4(d) arises only for sizes >4 nm. Figure 4(b) shows that for a short pause of 2 min, only the smaller particles from the first deposition had sunk into the film. This

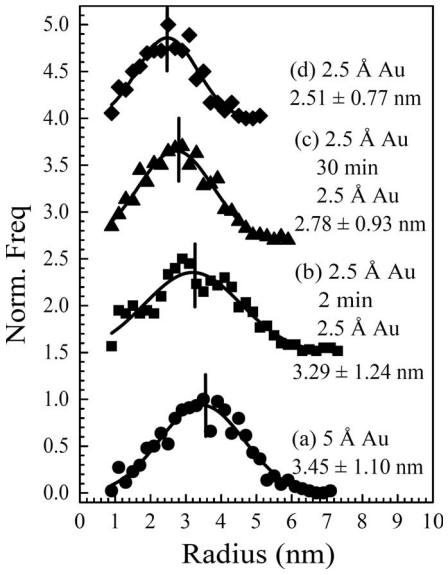

FIG. 4. Particle size distributions after deposition on 30 nm Bi films at room temperature. The deposition rate was 1 Å/min. The distributions are normalized and vertically displaced for clarity. The continuous lines are a guide to the eye. The deposition conditions and the average particle sizes are included (they are also marked on the plot). For a wait time of 2 min, the size distribution in (b) resembles (a), except at small sizes (1–2 nm). The wait time of 30 min in (c) allowed the particles to burrow and the size distribution resembles (d), despite the difference in the amount of material.

can be seen from the higher frequency of particles of size <2 nm in the distribution of Fig. 4(b) compared to Fig. 4(a). We conclude that burrowing time was >30 min for those with 4–5 nm radii (the largest obtained during the 2.5 Å deposition), while it was <2 min for those with 1–2 nm radii. Thus, the burrowing time is directly related to particle size (after some critical size that results in energy gain, for burrowing) with smaller particles burrowing faster than larger ones.

Figure 5 shows changes in particle sizes and densities as a function of substrate temperature during Au deposition. The Bi film was grown at room temperature and then heated to and held at the deposition temperature while Au was deposited at ~1 Å/min. Subsequently, the sample was cooled to room temperature and imaged *ex situ*. If there were no burrowing, an increase in temperature should lead to an increase in average particle size due to increased diffusivity. This trend is initially seen from 25 to 50 °C, but the average size then remains the same at 75 °C, with a broader distribution, and it decreases and narrows sharply at 100 °C.

This trend can be understood in terms of the relative changes to adatom diffusion and burrowing rates. The temperature dependence of the burrowing rate enters through the interface diffusion coefficient (δD). For the adatom diffusion rate, it enters through the Au surface diffusion on Bi (D_s), which can be estimated from the surface self-diffusion coefficients ($D_{\text{Au/Bi}}$) of the individual components,[21]

$$D_s = \sqrt{D_{\text{Au}} D_{\text{Bi}}},$$

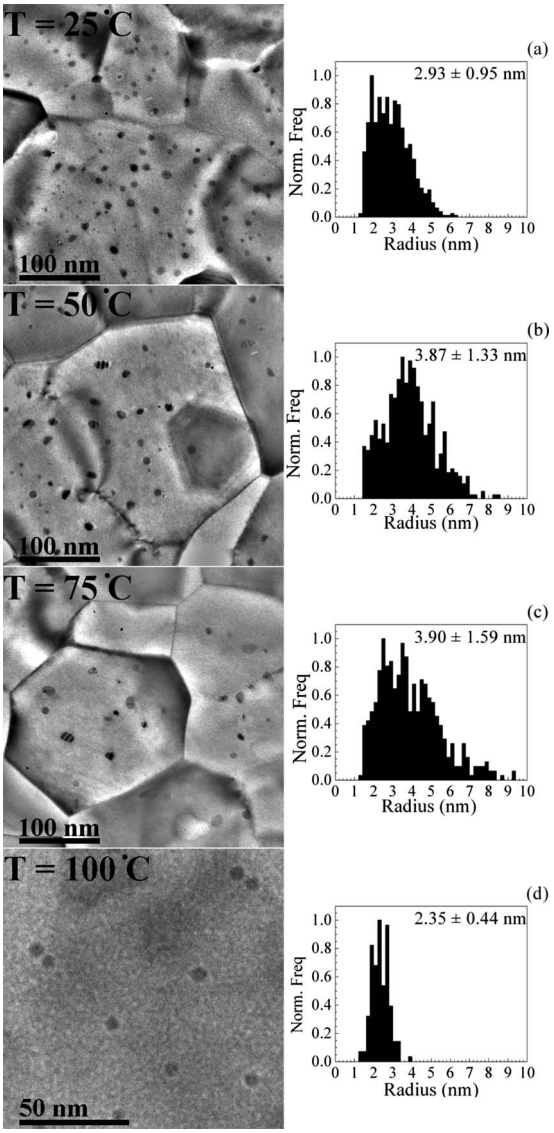

FIG. 5. Representative TEM images and size distributions for the same amount of Au deposited on Bi at different temperatures. The average particle size and size distribution increases for $T=50$ °C, broadens at 75 °C, and decreases for 100 °C. The distribution arises from the competition between adatom diffusion that forms the particles and burrowing that sinks them in the substrate. As the temperature rises, the higher diffusion and burrowing rates increase the average size and broaden the distribution. Once burrowing is dominant, there is a decrease in average size and a narrower distribution.

$$D_{\mathrm{Au}} = 1 \times 10^{-4} \exp\left(-5.9\frac{T_{m(\mathrm{Au})}}{T}\right) \mathrm{m}^2\ \mathrm{s}^{-1},$$

$$D_{\mathrm{Bi}} = 1.4 \times 10^{-6} \exp\left(-5.9\frac{T_{m(\mathrm{Bi})}}{T}\right) \mathrm{m}^2\ \mathrm{s}^{-1}, \qquad (4)$$

where $T_{m(\mathrm{Au/Bi})}$ is the bulk melting point. Since the interface diffusion coefficient has a higher exponent, its rate of increase with temperature is higher than surface diffusion. A higher burrowing rate causes more material to be buried as small particles. These particles would have sizes less than 1 nm, the smallest size seen in the TEM images because Bi has a higher atomic number than Au and hence a higher Z contrast. Thus, as more material is buried as small particles, there is a lower density of observable particles in Figs. 5(a)–5(d). Initially, fewer particles on the surface lead to larger sizes, Figs. 5(b) and 5(c). However, once the burrowing rate is much higher than diffusion, the size decreases because most of the material has buried as small particles, Fig. 5(d).

C. Simulation of particle formation

These experiments show that the particle formation is influenced by the relative rates of burrowing and surface diffusion. In order to gain greater insight into this process, we performed kinetic Monte Carlo simulations of particle growth that took burrowing into account. These were compared with simulations without burrowing to understand the role of burrowing on particle formation. We have also simulated the "pause" in the experiments by using a wait time in the simulations and the effects of increasing temperature by changing the burrowing rate relative to diffusion rate for the same flux. The simulations provide information on the final size distributions and the instantaneous particle densities in the system.

Simulations were performed on a two-dimensional square lattice with periodic boundary conditions. Adatom arrival was modeled by choosing random sites in the lattice to place the atoms. They were then allowed to hop to one of the four nearest-neighbor sites. When two atoms met or an atom arrived at a site containing a particle or when two particles came together by growing, a new particle was formed whose radius was obtained from the volume of initial components, complete coalescence. To avoid branching effects, this coalescence was assumed to be instantaneous and occurred for all radii. The center of the new particle was determined by the weighted center of mass of the original components. Once the new particle was formed, nearest-neighbor sites were checked and coalescence was allowed if the new particle overlapped with an existing particle or atom. This process was repeated until there were no other atoms or particles in the nearest-neighbor sites. Once particles reached a certain size, they were allowed to burrow into the substrate at a rate inversely proportional to the fourth power of the radius. When a particle was completely burrowed, it could no longer grow. Thus, burrowing acted to remove existing particles from the simulation. The time step in the simulation was determined as the inverse of the total rate of impingement, diffusion, and burrowing. At each step, one of these processes was chosen depending on their relative rate. The individual rates, and hence the time steps, were dynamically updated to keep track of particle formation, growth, and burrowing. The total time in our simulation was equal to the deposition time of 300 s (5 Å at 1 Å/min). A running count of the number and sizes of particles in the system (both burrowed and on the surface) and adatoms on the surface was maintained and constantly checked with total number of atoms deposited. Simulations without burrowing were similar

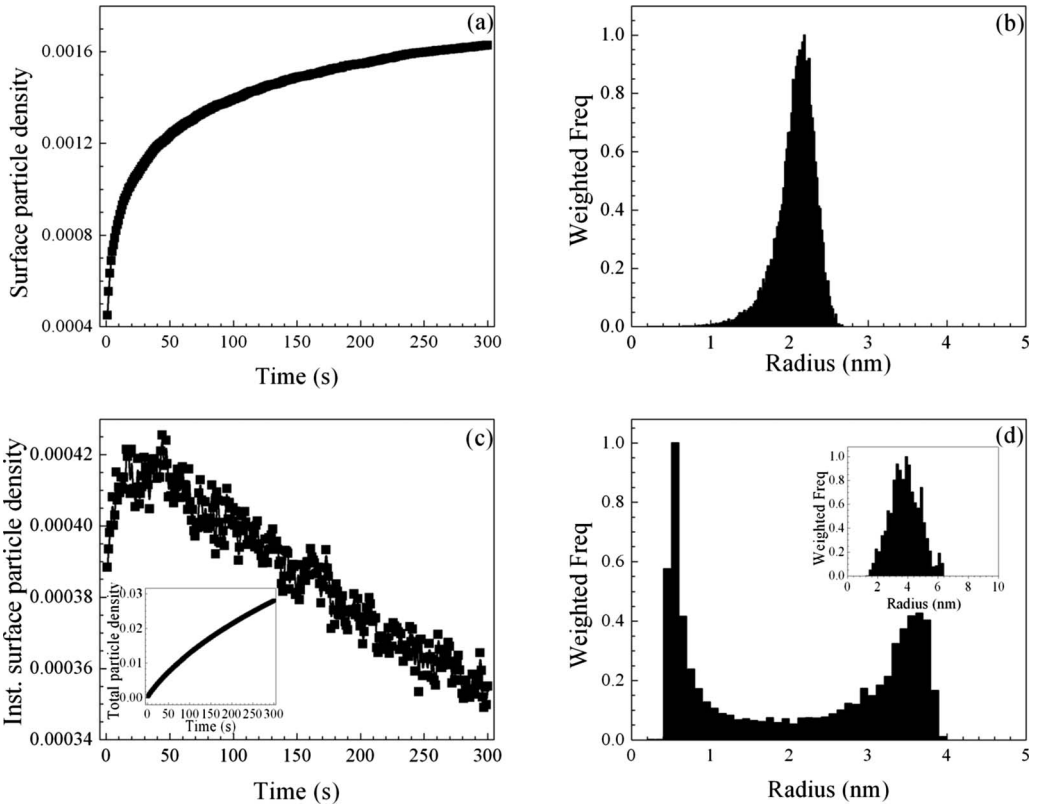

FIG. 6. Changes in particle density with time and weighted size distributions obtained from kinetic Monte Carlo simulations with and without burrowing. In (a), without burrowing, the surface particle density constantly increases with time. When there is burrowing, as in (c), the instantaneous surface particle density initially increases and then decreases. The total number of surface and buried particles increases linearly, as shown in the inset in (c). This is because formed particles constantly burrow, making available new sites for nucleation. Burrowing also leads to bimodal size distribution, seen in (d), compared to the size distribution without burrowing (b). The first peak corresponds to the critical size for burrowing while the second corresponds to those that remained on the surface during impingement. The inset in (d) is the weighted experimental size distribution.

except that there was no burrowing step and all the particles were on the surface.

The atom impingement rate (R_a) was calculated based on our experimental deposition rate of 1 Å/min or 0.01 ML/s multiplied by the area of the simulation lattice. The diffusion rate was estimated from the diffusion coefficient of Au on Bi (D_s) given in Eq. (4),

$$R_{\text{diff}} = \frac{4D_s}{l^2} N_A, \tag{5}$$

where l is the distance between lattice points, N_A is the instantaneous number of atoms on the surface, and the numerical factor is for two-dimensional isotropic diffusion. The rate of burrowing of particles was obtained by modifying Eq. (2) for the time required by particles to sink into the Bi film,

$$R_{\text{burr}} = \sum_{\substack{\text{particles} \\ \text{on surface}}} \left[\alpha \frac{kT}{V_m \gamma_{\text{Bi}} D_b} \left(V_{\text{Au}} \times s \times \frac{3}{4\pi} \right)^{4/3} \right]^{-1}, \tag{6}$$

where V_{Au} is the volume of one Au atom and s refers to the number of atoms in a particle. The rate was summed over all the particles that had not completely burrowed. These rates were used to determine the time step in the simulation and were dynamically updated.

As atoms aggregate to form clusters, they reach a size where they start sinking into the film. Density-functional studies of lowest-energy structures of Au show that the cluster shapes are flat for sizes less than 14 and become compact near spherical for larger sizes.[22] Burrowing occurs when the particles become spherical, and concepts such as surface and interface energy become valid. To this end, we varied the burrowing size in the simulation and calculated the amount of material that formed particles larger than 1 nm. For a burrowing size=25, this was 65%, which was close to the value of $70 \pm 10\%$ obtained from TEM images using the particle density and average volume. Hence we chose this size for our simulations. When the burrowing size was changed to 50 and 100 atoms, the amount changed to 62% and 64%, indicating a weak dependence on the burrowing size in the range 25–100 atoms.

Comparison of the final size distributions and number of particles with and without burrowing shows remarkable differences. These are summarized in Fig. 6, which is a plot of particle density vs time and weighted final size distributions. The weighted distributions were obtained by multiplying the number of particles with their volume. This is a direct mea-

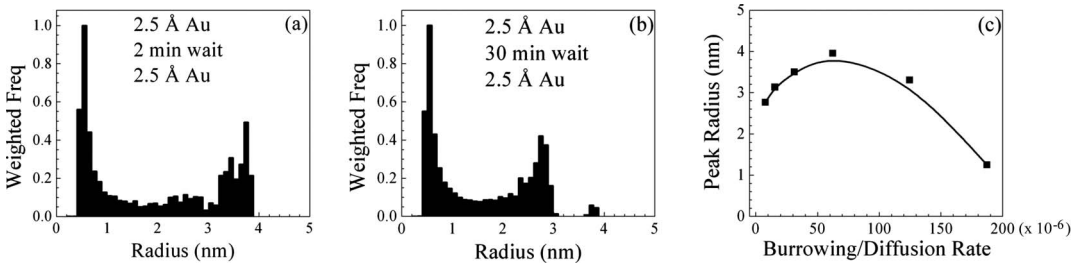

FIG. 7. Simulations of the pause experiments and temperature changes shown in Figs. 4 and 5. During the pause, no new atoms were deposited, but atoms remaining on the surface were allowed to diffuse. Particles on the surface and partially buried ones continued to burrow at a rate inversely proportional to the fourth power of their radius. The size distributions in (a) and (b) closely mimic the observed changes of Fig. 4 and described in Sec. III B. The plot of peak radius vs ratio of the burrowing and diffusion rate, shown in (c), can be compared with the results from Fig. 5. Initially, the size increases but it then decreases with increasing burrowing rates, mirroring changes activated by increasing temperature. The line acts as a guide to the eye.

sure of the amount of the material present as particles of a given size. Figures 6(a) and 6(b) show the plots without burrowing. They agree well with results obtained by conventional kinetic Monte Carlo simulations with single atom diffusion.[23,24] The plots shown in Figs. 6(c) and 6(d) keep the diffusion rate and flux the same but with a burrowing rate obtained from Eq. (6). In diffusion limited growth, as new particles nucleate, their number in the system increases. After a certain time, the arriving adatoms find existing particles rather than nucleating new ones, leading to a plateau in the density. For large enough coverages, the existing particles coalesce and this reduces their number. We are clearly in the plateau region at the end of our simulation in Fig. 6(a). With burrowing, as seen in Fig. 6(c), there are two major differences. First, the total particle density [sum of particles on the surface and buried, shown in the inset in Fig. 6(c)] is more than an order of magnitude higher than without burrowing. Second, this density increases almost linearly with no plateau region in this time interval.

A consequence of burrowing is that particles on the surface can grow larger than if there were no burrowing. Comparison of Figs. 6(b) and 6(d), which are the normalized weighted distributions without and with burrowing, shows that this is indeed the case. A bimodal size distribution with burrowing is seen. With burrowing, new particles constantly nucleate, leading to a linear increase in particle density. Most of these particles burrow once they reach the critical size and can no longer grow. This corresponds to the first peak in the size distribution. The second peak in the size distribution is from adatoms attaching to the particles remaining on the surface at each step, whose density slowly reduces with time, as seen in Fig. 6(c). Also, as a particle grows its burrowing rate drops since it is inversely dependent on the size. This means that there is a greater probability for newly formed small particles to burrow than the existing ones that are growing. These two effects lead to larger particles and a wider size distribution than without burrowing. The size distributions from the simulation can be qualitatively compared with the distribution seen in the experiments, e.g., Fig. 4(a). The experimental data are included as an inset in Fig. 6(d). The peak at lower radius in Fig. 6(d) occurs below 1 nm, and these particles are too small to be seen in TEM images due to contrast differences. The second peak occurs at 3.5 nm, which is close to the peak in the size distribution, seen in the inset. This agreement with experiment is very good despite the use of diffusivity data estimated from empirical relations based on the melting temperature.

We have also simulated the pause in the experiments by using a wait time in the simulations. During that time, remaining adatoms on the surface were allowed to diffuse until they met with an existing particle or nucleated a new one. Particles on the surface or partially sunk were allowed to burrow. The resulting size distributions in Figs. 7(a) and 7(b) match closely the experimental observations in Fig. 4. For a wait time of 2 min, only small particles have burrowed. The difference is evident in the size distributions around 2 nm from Figs. 4(b) and 7(a). For a wait time of 30 min, the initial particles have been buried and the distribution resembles the simulation for 2.5 Å Au (not shown).

We can simulate the effects of increasing temperature by increasing the burrowing rate relative to the diffusion rate for the same flux. In Fig. 7(c), we plot the radius corresponding to the second peak in the size distribution as a function of the ratio of the burrowing and diffusion rates. Increasing the burrowing rate initially increases the peak size, but the size starts to decrease with further increase in burrowing rate. This can be compared with changes seen in the size distributions in Fig. 5. Ultimately, in the limit of fast burrowing rates, particles can only reach the critical size for burrowing because they sink before the next atom arrives and attaches.

Deviations in size distributions from conventional diffusion have been seen for heteroepitaxial[25] and surfactant mediated growth.[26] For heteroepitaxial growth, a narrow size distribution was obtained due to accumulated strain in the islands. This causes atoms to detach from island edges so that once the islands of a certain size are formed they no longer grow. This leads to nucleation of new islands resulting in high density of small islands and a linear increase in island density with coverage (time). Simulations of aggregation, when particles above a certain size are removed from the system at a constant rate, also show a linear increase in island density with time.[27] For Ge on Si, a bimodal size distribution is seen during coarsening of particles.[28] This arises from the differences in chemical potential between pyramids and domes leading to different atom sticking coefficients. The effects of surfactant during growth of thin films have

been studied by using a kinetic tight-binding Ising model. These show that burrowing decreases with increasing deposition rates for a given substrate temperature.[26] Our results compare the rates of diffusion and burrowing for a given deposition rate and show that burrowing leads to a broadening in size distribution by constantly removing formed particles from the surface. This result is important to understand particle formation on low-energy substrates.

IV. CONCLUSION

We have shown that particle assembly for gold deposited on bismuth must take into account burrowing to explain the observed particle sizes. By recording the size distributions for various substrate temperatures, we have studied the effects of relative rates of diffusion and burrowing on particle formation. Kinetic Monte Carlo simulations that incorporate a burrowing rate on particle formation show that larger sized particles are obtained with burrowing compared to without burrowing. This counterintuitive result can be explained by the fact that small particles sink into the substrate hence particles remaining on the surface can grow easily. Burrowing should occur for systems where the surface energy of the deposited species is higher than the substrate. Knowledge of the kinetics of the process is important to understand nanostructure formation for these systems to decide appropriate deposition conditions.

ACKNOWLEDGMENTS

TEM and XRD measurements were carried out in the Frederick Seitz Materials Research Laboratory (FSMRL) Central Facilities, University of Illinois, which are partially supported by the U.S. Department of Energy under Grants No. DE-FG02-07ER46453 and No. DE-FG02-07ER46471. We thank Mauro Sardela of FSMRL for helping us with the XRD measurements.

[1] J. A. Venables, G. D. T. Spiller, and M. Hanbucken, Rep. Prog. Phys. **47**, 399 (1984).
[2] H. Brune, Surf. Sci. Rep. **31**, 125 (1998).
[3] J. W. Evans, P. A. Thiel, and M. C. Bartelt, Surf. Sci. Rep. **61**, 1 (2006).
[4] P. Jensen, Rev. Mod. Phys. **71**, 1695 (1999).
[5] C. G. Zimmermann, M. Yeadon, K. Nordlund, J. M. Gibson, R. S. Averback, U. Herr, and K. Samwer, Phys. Rev. Lett. **83**, 1163 (1999).
[6] S. Padovani, F. Scheurer, and J. P. Bucher, Europhys. Lett. **45**, 327 (1999).
[7] A. Rolland and B. Aufray, Surf. Sci. **162**, 530 (1985).
[8] P. J. Schmitz, W. Y. Leung, G. W. Graham, and P. A. Thiel, Phys. Rev. B **40**, 11477 (1989).
[9] M. Kamiko, H. Mizuno, H. Chihaya, J. H. Xu, I. Kojima, and R. Yamamoto, Appl. Surf. Sci. **252**, 364 (2005).
[10] M. Kamiko, H. Mizuno, J. H. Xu, I. Kojima, and R. Yamamoto, J. Cryst. Growth **263**, 363 (2004).
[11] M. Kamiko, H. Mizuno, H. Chihaya, J. H. Xu, I. Kojima, and R. Yamamoto, Jpn. J. Appl. Phys., Part 1 **43**, 3561 (2004).
[12] C. Servant, E. Zoro, and B. Legendre, CALPHAD: Comput. Coupling Phase Diagrams Thermochem. **30**, 443 (2006).
[13] C. V. Thompson, Annu. Rev. Mater. Sci. **20**, 245 (1990).
[14] M. De Graef, *Introduction to Conventional Transmission Electron Microscopy* (Cambridge University Press, Cambridge, England, 2003).
[15] J. Frantz and K. Nordlund, Phys. Rev. B **67**, 075415 (2003).
[16] L. Vitos, A. V. Ruban, H. L. Skriver, and J. Kollar, Surf. Sci. **411**, 186 (1998).
[17] R. A. Masumura, M. E. Glicksman, and C. L. Vold, Scr. Metall. **6**, 943 (1972).
[18] G. C. Hasson and C. Goux, Scr. Metall. **5**, 965 (1971).
[19] C. G. Zimmermann, K. Nordlund, M. Yeadon, J. M. Gibson, R. S. Averback, U. Herr, and K. Samwer, Phys. Rev. B **64**, 085419 (2001).
[20] A. M. Brown and M. F. Ashby, Acta Metall. **28**, 1085 (1980).
[21] E. G. Seebauer and C. E. Allen, Prog. Surf. Sci. **49**, 265 (1995).
[22] J. L. Wang, G. H. Wang, and J. J. Zhao, Phys. Rev. B **66**, 035418 (2002).
[23] M. C. Bartelt and J. W. Evans, Phys. Rev. B **46**, 12675 (1992).
[24] J. W. Evans and M. C. Bartelt, J. Vac. Sci. Technol. A **12**, 1800 (1994).
[25] A. L. Barabasi, Appl. Phys. Lett. **70**, 2565 (1997).
[26] J. M. Roussel, A. Saul, G. Treglia, and B. Legrand, Surf. Sci. **352-354**, 562 (1996).
[27] T. Vicsek, P. Meakin, and F. Family, Phys. Rev. A **32**, 1122 (1985).
[28] F. M. Ross, J. Tersoff, and R. M. Tromp, Phys. Rev. Lett. **80**, 984 (1998).